

WaterGAN: Unsupervised Generative Network to Enable Real-time Color Correction of Monocular Underwater Images

Jie Li¹, Katherine A. Skinner², Ryan M. Eustice³ and Matthew Johnson-Roberson³

Abstract—This paper reports on WaterGAN, a generative adversarial network (GAN) for generating realistic underwater images from in-air image and depth pairings in an unsupervised pipeline used for color correction of monocular underwater images. Cameras onboard autonomous and remotely operated vehicles can capture high resolution images to map the seafloor, however, underwater image formation is subject to the complex process of light propagation through the water column. The raw images retrieved are characteristically different than images taken in air due to effects such as absorption and scattering, which cause attenuation of light at different rates for different wavelengths. While this physical process is well described theoretically, the model depends on many parameters intrinsic to the water column as well as the objects in the scene. These factors make recovery of these parameters difficult without simplifying assumptions or field calibration, hence, restoration of underwater images is a non-trivial problem. Deep learning has demonstrated great success in modeling complex nonlinear systems but requires a large amount of training data, which is difficult to compile in deep sea environments. Using WaterGAN, we generate a large training dataset of paired imagery, both raw underwater and true color in-air, as well as depth data. This data serves as input to a novel end-to-end network for color correction of monocular underwater images. Due to the depth-dependent water column effects inherent to underwater environments, we show that our end-to-end network implicitly learns a coarse depth estimate of the underwater scene from monocular underwater images. Our proposed pipeline is validated with testing on real data collected from both a pure water tank and from underwater surveys in field testing. Source code is made publicly available with sample datasets and pretrained models.

Index Terms—Underwater vision, monocular vision, generative adversarial network, end-to-end model, image restoration

I. INTRODUCTION

Many fields rely on underwater robotic platforms equipped with imaging sensors to provide high resolution views of the seafloor. Marine archaeologists use photomosaic maps to study submerged objects and cities [1]; marine scientists use surveys of coral reef systems to track bleaching events over time [2]. While recent decades have seen great advancements in vision capabilities of underwater platforms, the subsea environment presents unique challenges to perception that are not present on land. Range-dependent lighting effects

¹ J. Li is with the Department of Electrical Engineering and Computer Science, University of Michigan, Ann Arbor, MI 48109 USA ljlijie@umich.edu

² K. Skinner is with the Robotics Program, University of Michigan, Ann Arbor, MI 48109 USA kskin@umich.edu

³ R. Eustice and M. Johnson-Roberson are with the Department of Naval Architecture and Marine Engineering, University of Michigan, Ann Arbor, MI 48109 USA mattjnr@umich.edu

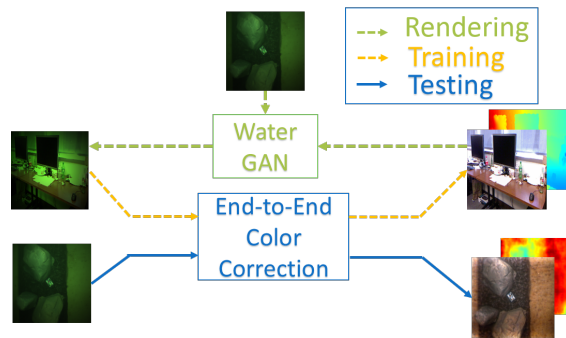


Fig. 1: System flowchart displaying both the GAN network and the end-to-end color correction network proposed.

such as attenuation cause exponential decay of light between the imaged scene and the camera. This attenuation acts at different rates across wavelengths and is strongest for the red channel causing raw underwater images to appear relatively blue or green compared to the true color of the scene as it would be imaged in air. Simultaneously, light is added back to the sensor through scattering effects causing a haze effect reducing effective resolution. Lastly, many real-time depth sensors common in terrestrial vision applications fail in underwater environments particularly at long ranges due to these complex properties of light propagation underwater. In recent decades, stereo cameras have been at the forefront in solving these challenges. With calibrated stereo pairs, high resolution images can be aligned with depth information to compute large-scale photomosaic maps or metrically accurate 3D reconstructions [3]. However, degradation of images due to range-dependent underwater lighting effects still hinders these approaches, and restoration of underwater images involves reversing effects of a complex physical process with prior knowledge of water column characteristics for a specific survey site.

Alternatively, neural networks can achieve end-to-end modeling of complex nonlinear systems. Yet deep learning has not become as commonplace subsea as it has for terrestrial applications. One challenge is that many deep learning structures require large amounts of training data, typically paired with labels or corresponding ground truth sensor measurements. Gathering large sets of underwater data with depth information is challenging in deep sea environments; obtaining ground truth of the true color of a natural subsea scene is also an open problem.

Rather than gathering this data, we propose a novel approach, WaterGAN, a generative adversarial network

(GAN) [4] that takes in-air images and depth maps as input and generates corresponding synthetic underwater images, using real unlabeled underwater images to learn a realistic representation of water column properties of a particular survey site. This model can then supplant the need for real ground truth depth and color in the training of an end-to-end color correction network. That network can then take as input raw unlabeled underwater images to output restored images that appear as if they were taken in air. The underwater environment offers an advantage over terrestrial imaging for this problem domain. We show how the underwater attenuation process in fact enables the monocular recovery of relative depth given the implicit information encoded in the range-based attenuation effects. Thus our proposed network can learn a coarse monocular depth estimator as well as an end-to-end model for image restoration of monocular underwater images.

This paper is organized as follows: §II presents relevant prior work; §III gives a detailed description of our technical approach; §IV validates the proposed approach using real data presenting both experimental setup and results; finally, §V and §VI provide discussion and conclusion, respectively.

II. BACKGROUND

Prior work on compensating for effects of underwater image formation has focused on explicitly modeling this physical process to restore underwater images to their true color. Jordt et al. rely on a simplified model with parameters obtained through prior experiments [5]. Several methods have addressed range-dependent image dehazing by estimating depth through developed or statistical priors on attenuation effects [6], [7], [8]. However, attenuation parameters vary for each survey site depending on water composition and quality, as well as lighting patterns from ambient light, sunlight or direct lighting sources on the survey platform. Bryson et al. uses an optimization approach to account for vehicle lighting configuration, solving for true color of underwater scenes using real data. [9]. However, this method requires detailed knowledge of vehicle configuration and camera pose relative to the scene. In this paper we propose to learn to model these effects using a deep learning framework without explicitly encoding vehicle configuration parameters. Other methods for underwater image restoration exist that do not rely on an explicit physical model. Such approaches include simple techniques like normalizing using the greyworld assumption [1], and histogram equalization. Both are common preprocessing steps for underwater images and result in improved image quality and color. However, as such methods have no knowledge of range-dependent effects, they are not suitable for environments with large depth variation. Work has been done to enforce the consistency of restored images across a scene [10], but these methods require depth maps. In prior work the authors have worked to relax this requirement using an underwater bundle adjustment formulation to estimate the parameters of a fixed attenuation model and the 3D structure simultaneously [11], but

such approaches require a fixed image formation model and handle unmodeled effects poorly. The approach presented here can perform restoration with single shot monocular images as input, and learns the structure of the scene as it corrects for the effects of range-dependent attenuation.

More recent work has been focusing on leveraging the success in end-to-end modeling of deep learning techniques to estimate the complicated physical model. Cho et al. [12] develop a deep learning pipeline for underwater image dehazing using simulated data. Their work achieves state-of-art dehazing performance by estimating ambient light and a transmission map through a convolution network in a patch-based manner. However, they do not address attenuation or color correction. The lack of real training data makes it hard to use these types of supervised methods in the application of color correction in that attenuation coefficients are different under different environments. Additionally, the patch-based parameter estimation limits the processing speed for one single image. In this work, we would like to overcome the problem of a lack of ground truth data by generating realistic data that captures the underlying physical model of underwater image formation. Based on this, we propose a dense, end-to-end model learning framework that results in pixel-wise color correction for a whole image in a single network. Thus our framework is deployable in real-time systems.

We structure our training data generator, WaterGAN, as a generative adversarial network (GAN). GANs have shown success in generating realistic images in an unsupervised pipeline that only relies on an unlabeled set of images of a desired representation [4]. A standard GAN generator receives a noise vector as input and generates a synthetic image from this noise through a series of convolutional and deconvolutional layers [13]. Wang and Gupta incorporate both structural information (normals) and initial imagery into their generator network to generate more realistic images based on physical structure of a scene [14]. However, their discriminator network relies on ground truth normal data to ensure that the generator learns the relationship between structure and color. Since our goal is to restore monocular images, we do not have depth maps of real data as input to the discriminator. Instead, we structure the generator network to use depth information paired with in-air images in a way that mimics the model for underwater light propagation. Sixt et al. propose a related approach in RenderGAN, a framework for generating training data for the task of tag recognition in cluttered images [15]. RenderGAN uses an augmented generator structure with augment functions modeling known characteristics of their desired images, including blur and lighting effects. RenderGAN focuses on a finite set of tags and classification as opposed to a generalizable transmission function and image-to-image mapping.

III. TECHNICAL APPROACH

This paper presents a two-part technical approach ultimately producing a trained network that enables novel

monocular imagery to be color corrected and dehazed. Figure 1 shows an overview of our full pipeline. WaterGAN is the first component of this pipeline, taking as input in-air RGB-D images (which are trivial to gather) to train a generative network adversarially. This training procedure uses non-corresponding unlabeled raw underwater images of a specific survey site, under the assumption that the water column effects close to the benthos are mostly uniform in a small local area. Such assumptions can be relaxed by training multiple models for different latitude and longitude locations within a single site. This process produces rendered underwater images from in-air RGB-D images that conform to the characteristics of the real underwater data at that site. These synthetic underwater images can then be used to train the second component of our system, a novel end-to-end network that can correct for water column effects in a specific location in real-time.

A. Generating Realistic Underwater Images

We structure WaterGAN as a generative adversarial network, which has two networks training simultaneously: a generator, G , and a discriminator, D (Fig. 2).

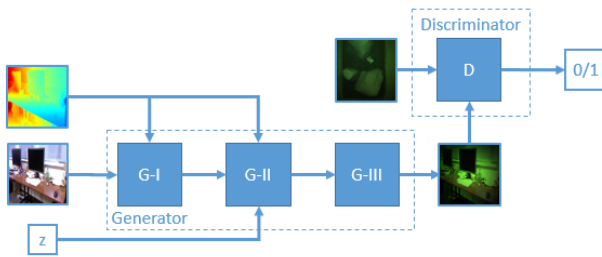


Fig. 2: WaterGAN: The GAN for generating water column attenuated images with similar image formation properties to those of unlabeled underwater data taken in the field.

In a standard GAN [4] [13], the generator input is a noise vector z , which is projected, reshaped, and propagated through a series of convolution and deconvolution layers. The output is a synthetic image, $G(z)$. The discriminator receives as input the synthetic images and a separate dataset of real underwater images, x , and classifies each sample as real (1) or synthetic (0). The goal of the generator is to output synthetic images that the discriminator classifies as real. Thus in optimizing G , we seek to maximize

$$\log(D(G(z))) \quad (1)$$

The goal of the discriminator is to achieve high accuracy in classification, minimizing the above function, and maximizing $D(x)$ for a total value function of

$$\log(D(x)) + \log(1 - D(G(z))) \quad (2)$$

We have created a novel generator network for WaterGAN that receives input RGB-D data gathered terrestrially, along with a noise vector. The value functions for the generator and discriminator, respectively, become:

$$\log(D(G(I_{air}, r_c, z))) \quad (3)$$

$$\log(D(x)) + \log(1 - D(G(I_{air}, r_c, z))) \quad (4)$$

where I_{air} is the input in-air image, and r_c is the range from the camera to the scene.

The generator of WaterGAN features three main stages, each modeled after a component of underwater image formation: attenuation (G-I), scattering (G-II), and vignetting (G-III). The purpose of this structure is to ensure that generated images align with RGB-D input, such that each stage does not alter the structure or texture of the scene itself only its relative color and intensity. Additionally, our formulation ensures that the network is using depth information in a realistic manner. This is necessary as the discriminator does not have direct knowledge of the depth of scene. This is a deliberate choice enabling the correction of underwater imagery without explicit depth information. The remainder of this section describes each stage in detail.

G-I: Attenuation

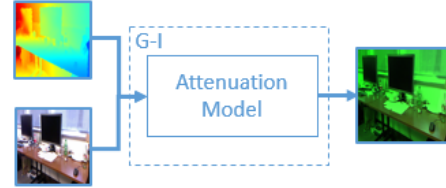


Fig. 3: Generator: attenuation layers

The first stage of the generator, G-I, accounts for range-dependent attenuation of light. The attenuation model is a simplified formulation of the Jaffe-McGlamery model [16] [17]:

$$G_1 = I_{air} e^{-\eta(\lambda)r_c} \quad (5)$$

where I_{air} is the input in-air image, or the initial irradiance before propagation through the water column, r_c is the range from the camera to the scene, and η is the wavelength-dependent absorption coefficient estimated by the network. G_1 is the final output of G-I, the final irradiance subject to attenuation in the water column. Note that the attenuation coefficient is dependent on water composition and quality, and varies across survey sites. To ensure that this stage only attenuates light and that the coefficient stays within reasonable physical bounds, we constrain η to be between 0 and 1. All input depth maps and images have dimensions of 64x64 for training. Depth maps for in-air training data are normalized to the max underwater survey altitude expected. Given the limits of optical surveys (there are altitudes for which imaging is impossible) there are reasonable values for this normalization assumption in almost all cases.

G-II: Scattering

As a photon of light travels through the water column it is also subjected to scattering back toward the image sensor.

This creates a characteristic haze effect in underwater images and is modeled by

$$B(\lambda) = \beta(\lambda)(1 - e^{-\eta(\lambda)r_c}) \quad (6)$$

where β is a scalar parameter dependent on wavelength. Stage G-II accounts for scattering through a shallow convolutional network shown in Fig. 4.

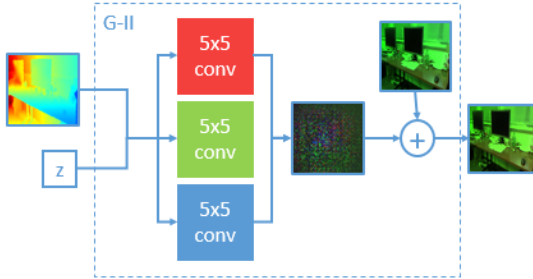


Fig. 4: Generator: scattering layers

To capture range-dependency, we input the 64x64 depth map and a 100-length noise vector. The noise vector is projected, reshaped, and concatenated to the depth map as a single channel 64x64 mask. To capture wavelength-dependent effects, we copy this input for three independent convolution layers with kernel size 5x5 and standard deviation of 0.02. This output is batch normalized and put through a final leaky rectified linear units (LReLU) with a leak rate of 0.2. Each of the three outputs of the distinct convolution layers are concatenated together to create a 64x64x3 dimension mask. Since scattering adds light back to the image, and to ensure that the structure of the image is not changed from the RGB-D input, we add this mask, M_2 to the output of G-I.

$$G_2 = G_1 + M_2 \quad (7)$$

G-III: Vignetting

Lastly we model vignetting, which produces a shading pattern around the borders of an image due to effects from the lens.



Fig. 5: Generator: vignetting layers

We adopt a simple vignetting model using a scaled spatial Gaussian filter

$$M_3 = A \frac{1}{2\pi\sigma^2} e^{-\frac{x^2+y^2}{2\sigma^2}} \quad (8)$$

where A is a scaling factor estimated by the network, σ is assumed constant at 2.2, and x and y are spatial coordinates of the kernel filter. The output mask has dimensions of the

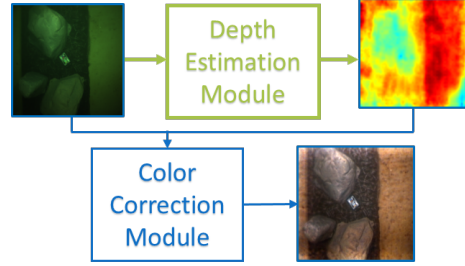


Fig. 6: Overview of two-module end-to-end monocular color correction pipeline. Module 1 estimates depth from underwater images using the information encoded in attenuation, and module 2 takes that estimated depth and inverts the underwater image formation process.

input images, and is multiplied by G_2 to produce a vignetted image G_3 .

$$G_3 = M_3 G_2 \quad (9)$$

For the discriminator of WaterGAN, we adopt the convolutional network structure used in [13]. The discriminator takes an input image 64x64x3, real or synthetic. This image is propagated through four convolutional layers with kernel size 5x5 and standard deviation of 0.02, with the image dimension downsampled by a factor of two and the channel dimension doubled. Each convolutional layer is followed by LReLUs with a leak rate of 0.2. The final layer is a sigmoid function and the discriminator returns a classification label.

B. End-to-end Model Learning

To perform real-time monocular image color correction, we propose a two-stage algorithm using two fully convolutional network modules trained on rendered underwater images generated by WaterGAN, and corresponding in-air RGB-D images. A basic pipeline is depicted in Fig. 6. A depth estimation module first reconstructs a coarse depth map from the input underwater image. Then a color correction module performs restoration based on the underwater image and its estimated depth map.

To provide pixel-wise estimation, we design the basic architecture of each module based on a state-of-the-art fully convolutional encoder-decoder network for end-to-end dense learning, called SegNet [18]. The illustration of the basic architecture is given in Fig. 7. The encoder network consists of 9 convolution layers followed by rectified linear units (ReLU) and 3 max-pooling layers for downsampling. In the decoder, we use the upsample layers proposed in SegNet. This approach uses indices from corresponding max-pooling layers that requires no learning in upsample steps.

We expand this basic architecture to compensate for the loss in high frequency components through the network by forward feeding the full resolution input into the output of the decoder to refine the final output of the network. We call this a resolution refinement layer. Alternative approaches to address this problem have been proposed previously where two networks at different resolutions are combined with the

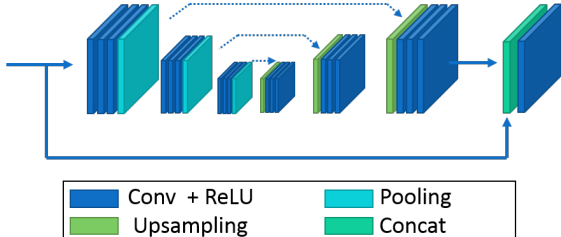


Fig. 7: Basic network architecture for both depth estimation and color correction modules.

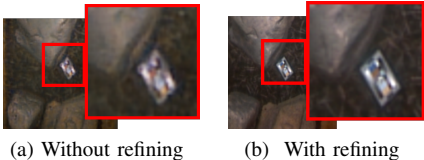


Fig. 8: Color correction results with and without resolution refinement layer. Note the improved spatial resolution on the color calibration target.

same goal of increasing output resolution [19]. Qualitative experiments indicate that our resolution refinement layer improves the proposed network performance by preserving more high frequency information from the input images. A sample of the color correction output is shown in Fig. 8, where results after convergence, both with and without the refinement layer are shown. Note that the resolution refinement layer also improves the network convergence speed in addition to increasing spatial resolution.

The depth estimation module takes an RGB input of $56 \times 56 \times 3$ with an output depth map of $56 \times 56 \times 1$. This map is then upsampled to 224×224 and serves as the input to the second stage: the color correction module. This module captures the inverse light propagation process. Given an RGB image and the estimated depth map, it produces a corrected color image of $224 \times 224 \times 3$. Euclidean loss is the final layer for both the color correction and the depth estimation modules. It should be noted that while the process described here is a two-stage process, providing color correction through monocular depth estimation, if accurate depth information is available from another source (e.g. from stereo) this information can be fed into the second module to perform color correction directly using this metric information.

IV. EXPERIMENTS & RESULTS

We evaluate our proposed method using several different underwater datasets, including surveys of an artificial testbed and several surveys of images collected in the field. As input RGB-D for all experiments, we compile three indoor Kinect datasets (B3DO [20], UW RGB-D Object [21] and NYU Depth [22]) for a total of 5349 RGB-D images.

A. Artificial Testbed

The first survey is done using a man-made rock platform submerged in a pure water test tank at University of Michigan's

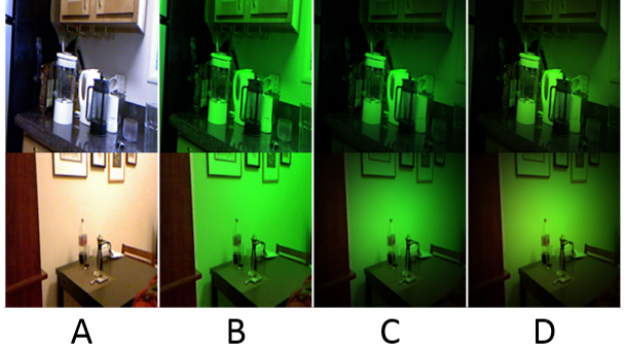


Fig. 9: Air images rendered using the generator trained on as if taken in the MHL tank water column. A is the original image, B is with attenuation applied, C with attenuation and vignetting, and D with attenuation, vignetting, and scattering.

Marine Hydrodynamics Laboratory (MHL). The rock platform is 4 ft x 7 ft large with rocks standing approximately 3 ft off the platform to give sufficient variation in depths for our testing. The platform base is covered in textured mesh. Figure 12d shows the platform imaged in air. A total of over 7000 underwater images were compiled from this survey to test our proposed method for color correction.

We use these images as real samples for input to WaterGAN's discriminator network. We train WaterGAN on a Titan X (Pascal) with 5000 RGB-D and 5000 underwater images with a batch size of 64 images and a learning rate of 0.0002. Through experiments, we found 25 epochs to be sufficient to render realistic images for input to the color correction network. Experiments with over 100 epochs showed overfitting such that the generator learned to trick the discriminator with noise patterns. Note that although we train WaterGAN on image sizes of 64x64x3, the network structure is capable of outputting higher resolution images by upsampling learned masks. The main limitation for training on high resolution images is GPU memory, not network architecture. Figure 9 shows sample images generated by our network where (A) shows the in-air image, (B) shows the rendered image with attenuation only, (C) shows the image with simulated attenuation and vignetting, and (D) shows the final image with the complete generator.

Next, we train our proposed end-to-end correction model with our generated data and corresponding RGB-D images. A total of 5349 rendered underwater images were generated for each experiment. We split this set into a training set with 4850 images and a validation set with 499 images. Since the network is fully convolutional, we can use this architecture for any size input, but are limited by the memory of our machine. Thus we train the network with downsampled images of size 112×112 and a batch size of 20, with a base learning rate of $1e-6$ and a momentum of 0.9. On a Titan X (Pascal) GPU, the depth estimation module takes around 11 hours to converge, while the color correction network takes approximately 25 hours to converge. Note that once a full model is learned, we can perform transfer learning to adapt the model to datasets from different underwater surveys,

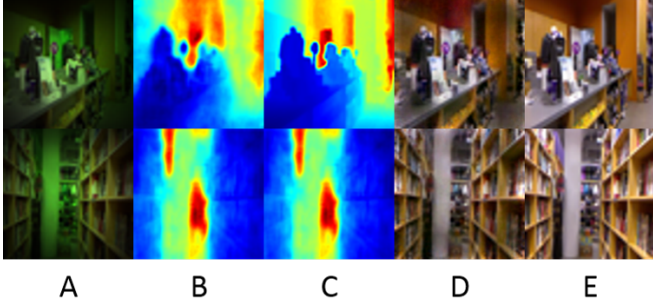


Fig. 10: Model validation tests showing that the (A) rendered underwater image can be used to produce (B) the estimated depth and it matches (C) the true depth. Also (D) the estimated in-air image and (E) the real in-air image are also closely matched.

shortening training time to approximately 1 hour. Testing on our trained network can be performed in real-time on a GPU. In our timing experiments, the forward propagation for depth estimation takes 0.007s on average and the color correction module takes 0.01s on average. With CPU only, the depth estimation takes 0.02s and color correction takes 0.15s, which still achieves frame-rate processing speed for most underwater vision surveys.

Figure 10 shows examples of validation tests on generated images, where (A) is the rendered underwater image, (B) is the estimated depth, (C) shows the true depth, (D) presents estimated in-air color, and (E) shows the original in-air image. These validation results indicate that the network is able to learn the underlying model encoded in the training data, and that our end-to-end modeling network can produce a promising restoration result on the validation data.

Test results using the MHL dataset with the proposed network are shown in Fig. 11 as follows: (A) raw images, (B) estimated depth, (C) our model with attenuation only, (D) our model with attenuation and vignetting, and (E) final results of our proposed model accounting for attenuation, scattering, and vignetting.

Here we can see the effects of modeling each component of underwater image formation in our generative network. Between (C) and (D), now that our generator models vignetting, the restored images have reduced vignetting effects and higher quality as the model has a better understanding of the lighting pattern of the image. The convolution layer has the effect of dehazing, which is seen between images (D) and (E), where the images in (E) are brighter and clearer. Since this is an artificial setup, we know the maximum range of the scene from the camera, approximately 3.26m, so we use this information in our depth normalization process to give optimal results for estimated depth maps. We note that our model does not capture all effects, especially edge effects, which could perhaps be captured by adding complexity to the generator. However, given that these results are achieved with monocular images in real-time, this is very promising for many applications relying on vision of underwater robotic platforms to view the seafloor.

Lastly we compare our method to a correction method that

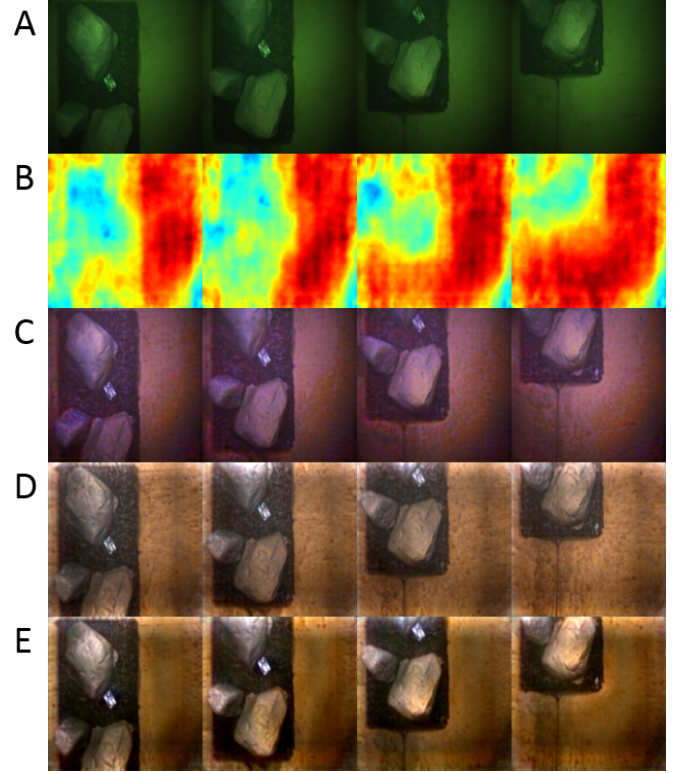


Fig. 11: Results showing color correction on the MHL dataset where each column shows (A) raw images, (B) estimated depth, (C) our model with attenuation only, (D) our model with attenuation and vignetting, and (E) final results on different images from the dataset.

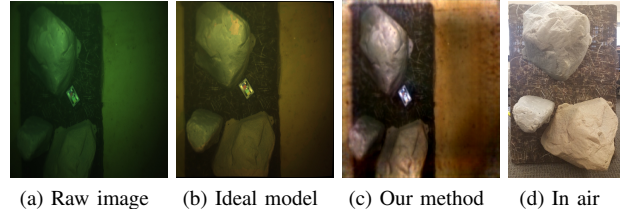


Fig. 12: Results comparing the raw underwater image (a), a comparison method using ideal attenuation coefficients for correction (b), our method (c), and the platform imaged in air (d).

models attenuation using generic water column parameters experimentally derived in the literature [16]. Figure 12 shows a comparison with the raw underwater image, the corrected image using the ideal attenuation model, our method, and the in-air image. Our method better corrects for vignetting and haze effects, showing a clearer scene in the resulting image. Additionally, we note that the ideal model relies on depth information for color correction which is not required for our proposed approach.

B. Field Tests

We also show results on two datasets collected in field experiments. The first dataset was collected in Port Royal, Jamaica in 2015, at the site of a submerged city in a depth

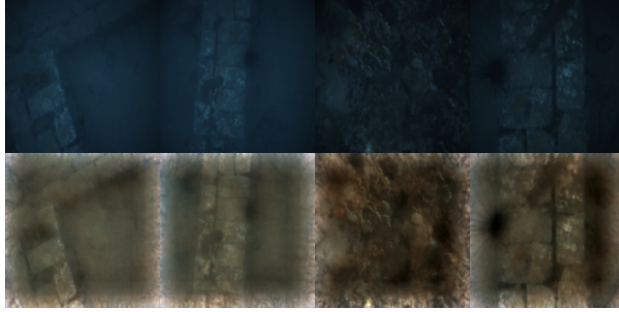


Fig. 13: Color correction for Port Royal dataset

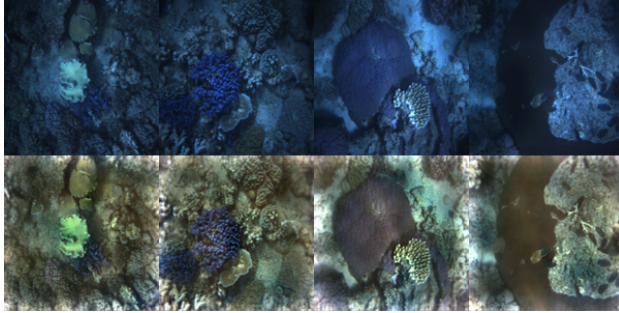


Fig. 14: Color correction for Lizard Island dataset

of 3-4 meters below the surface and contains both natural and man-made structure. These images were collected with a hand-held diver rig mounted with high resolution stereo cameras and the dataset consists of 6500 images from different dives in a local area. We assume the maximum distance is approximately 1.5m from the seafloor. Results for our color correction pipeline are shown in Fig. 13, with a sample depth estimate shown in Fig. 16.

Tests of our network on field data show interesting results when we break down the model into different components. Figure 15 shows rendered underwater images and corrected images from different models, where (a) models attenuation and vignetting only, and (b) models attenuation, vignetting, and scattering.

These results validate our approach to model scattering in our generator framework as the model without scattering does not sufficiently restore the real field data. This was less noticeable in the MHL test set because in pure water, at longer range, attenuation is the dominant lighting effect and there are small amounts of particulate matter in the water to

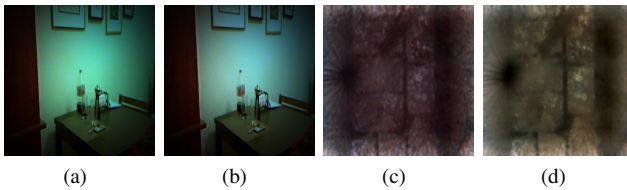


Fig. 15: Color correction results with (a) and (b) being training data for field data (c) and (d) with the latter of both pairs modeling scattering as well as attenuation and vignetting.

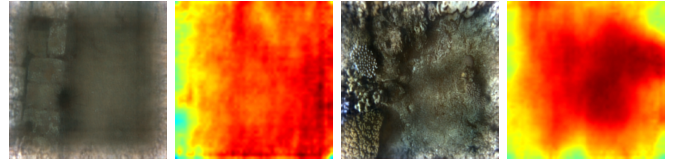


Fig. 16: Example results in depth estimation from two sites (a) and (c).

cause scattering. However, this field data is taken in saltwater environments at closer ranges, so the effects of attenuation are minimized, and scattering takes over as the dominant lighting effect for underwater image formation.

Our final dataset was collected at a coral reef system near Lizard Island, Australia. The data was gathered with the same diver rig and we assumed a maximum depth of 1.2m from the seafloor. A total number of 6083 images were compiled from the multi-dive survey. Figure 14 shows the results of our image restoration network, while Fig. 16 shows a sample depth estimate of a small area of the reef.

The depth estimation using real underwater data is less ideal than the validation result and the MHL survey of an artificial scene, but we are still able to discern coarse differences in depth, such as over a wall segment in Port Royal. Additionally, it is notable that the network is able to estimate a reasonable depth for the Lizard Island dataset, where most of the features are from natural scenes that are very different from the indoor scenes used for our training data. Ultimately, for all three datasets, the network is able to achieve consistent color correction and coarse depth map estimation in real-time.

V. DISCUSSION

Using WaterGAN as a generative network for modeling the complex physical process of underwater image formation, we are able to generate sufficient amounts of training data to train an end-to-end network to perform this correction. We note a few points raised during training of WaterGAN. Like many GAN architectures, there is a challenge to strike balance between training of the generator and discriminator. We updated the generator twice for every time we optimized the discriminator to aid in this training challenge. Additionally, developing specific stopping criteria for WaterGAN will improve our approach. We ran all experiments with 25 epochs, which gave good results for our proposed pipeline, but further experiments are needed to determine the optimal configuration for training the WaterGAN network.

As noted in [15], augmented generators may be limited in their ability to fully capture all aspects of a complex nonlinear model. We introduce a convolutional layer into our augmented generator that is meant to capture scattering, but we would like to experiment with adding additional layers to this stage for capturing more complex effects, such as lighting patterns from sunlight in shallow water surveys. Additionally, our end-to-end model is a fully convolutional

network that can take any size input. Our only limitation in obtaining higher resolution output is the memory capability of our system, but we would like to explore new ways of increasing the output resolution of the network.

Source code, sample datasets, and pretrained models are available at <https://github.com/kskin/WaterGAN>.

VI. CONCLUSIONS

This paper proposed WaterGAN, a generative network for modeling underwater images from RGB-D in air. We showed a novel generator network structure that incorporates the process of underwater image formation to generate high resolution output images and then adapted an end-to-end model learning pipeline for the task of color correction of monocular underwater images trained on RGB-D pairs and corresponding generated images. We showed that due to range-dependent effects inherent to the process of underwater image formation, and with training data of ground truth depth and underwater pairs, it is possible to learn to estimate a coarse depth map from only monocular underwater images as input.

ACKNOWLEDGMENTS

The authors would like to thank the Marine Hydrodynamics Laboratory at the University of Michigan for providing access to testing facilities, Eduardo Iscar and Jeffery Hsu for their help in collecting data, and Alexandra Carlson and Arash Ushani for insightful discussions. This work was supported in part by the National Science Foundation under Award Number: 1452793, the Office of Naval Research under award N00014-16-1-2102, and by the National Oceanic and Atmospheric Administration under award NA14OAR0110265.

REFERENCES

- [1] M. Johnson-Roberson, M. Bryson, A. Friedman, O. Pizarro, G. Troni, P. Ozog, and J. C. Henderson, "High-resolution underwater robotic vision-based mapping and 3d reconstruction for archaeology," *Journal of Field Robotics*, 2016.
- [2] M. Bryson, M. Johnson-Roberson, O. Pizarro, and S. Williams, "Automated registration for multi-year robotic surveys of marine benthic habitats," in *IEEE/RSJ International Conference on Intelligent Robots and Systems*, 2013.
- [3] M. Johnson-Roberson, M. Bryson, B. Douillard, O. Pizarro, and S. B. Williams, "Out-of-core efficient blending for underwater georeferenced textured 3d maps," in *IEEE Computing for Geospatial Research and Application (COM. Geo)*, 2013 Fourth International Conference on, pp. 8–15, 2013.
- [4] I. Goodfellow, J. Pouget-Abadie, M. Mirza, B. Xu, D. Warde-Farley, S. Ozair, A. Courville, and Y. Bengio, "Generative adversarial nets," in *Advances in Neural Information Processing Systems 27* (Z. Ghahramani, M. Welling, C. Cortes, N. D. Lawrence, and K. Q. Weinberger, eds.), pp. 2672–2680, Curran Associates, Inc., 2014.
- [5] A. Jordt, *Underwater 3D Reconstruction Based on Physical Models for Refraction and Underwater Light Propagation*. No. 2014/2 in Kiel Computer Science Series, Department of Computer Science, CAU Kiel, 2014. Dissertation, Faculty of Engineering, Kiel University.
- [6] N. Carlevaris-Bianco, A. Mohan, and R. M. Eustice, "Initial results in underwater single image dehazing," in *Proceedings of the IEEE/MTS OCEANS Conference and Exhibition*, (Seattle, WA, USA), pp. 1–8, September 2010.
- [7] P. Drews, Jr., E. do Nascimento, F. Moraes, S. Botelho, and M. Campos, "Transmission estimation in underwater single images," in *The IEEE International Conference on Computer Vision (ICCV) Workshops*, June 2013.
- [8] P. D. Jr., E. R. Nascimento, S. S. C. Botelho, and M. F. M. Campos, "Underwater depth estimation and image restoration based on single images," *IEEE Computer Graphics and Applications*, vol. 36, no. 2, pp. 24–35, 2016.
- [9] M. Bryson, M. Johnson-Roberson, O. Pizarro, and S. B. Williams, "True color correction of autonomous underwater vehicle imagery," *Journal of Field Robotics*, 2015.
- [10] M. Bryson, M. Johnson-Roberson, O. Pizarro, and S. Williams, "Colour-Consistent Structure-from-Motion Models using Underwater Imagery," in *Robotics: Science and Systems (RSS)*, 2012.
- [11] K. A. Skinner, E. I. Ruland, and M. J.-R. Johnson-Roberson, "Automatic color correction for 3d reconstruction of underwater scenes," in *IEEE International Conference on Robotics and Automation*, 2017. accepted.
- [12] Y. Cho, Y.-S. Shin, and A. Kim, "Online depth estimation and application to underwater image dehazing," in *OCEANS 2016 MTS/IEEE Monterey*, pp. 1–7, Sept 2016.
- [13] A. Radford, L. Metz, and S. Chintala, "Unsupervised representation learning with deep convolutional generative adversarial networks," *arXiv preprint arXiv:1511.06434*, 2015.
- [14] X. Wang and A. Gupta, *Generative Image Modeling Using Style and Structure Adversarial Networks*, pp. 318–335. Cham: Springer International Publishing, 2016.
- [15] L. Sixt, B. Wild, and T. Landgraf, "Rendergan: Generating realistic labeled data," *CoRR*, vol. abs/1611.01331, 2016.
- [16] J. S. Jaffe, "Computer modeling and the design of optimal underwater imaging systems," *IEEE Journal of Oceanic Engineering*, vol. 15, no. 2, pp. 101–111, 1990.
- [17] B. L. McGlamery, "Computer analysis and simulation of underwater camera system performance," tech. rep., UC San Diego, 1975.
- [18] V. Badrinarayanan, A. Kendall, and R. Cipolla, "Segnet: A deep convolutional encoder-decoder architecture for scene segmentation," *IEEE Transactions on Pattern Analysis and Machine Intelligence*, vol. PP, no. 99, pp. 1–1, 2017.
- [19] D. Eigen, C. Puhrsch, and R. Fergus, "Depth map prediction from a single image using a multi-scale deep network," in *Advances in neural information processing systems*, pp. 2366–2374, 2014.
- [20] A. Janoch, S. Karayev, Y. Jia, J. T. Barron, M. Fritz, K. Saenko, and T. Darrell, "A category-level 3-d object dataset: Putting the kinect to work," in *2011 IEEE International Conference on Computer Vision Workshops (ICCV Workshops)*, pp. 1168–1174, Nov 2011.
- [21] K. Lai, L. Bo, and D. Fox, "Unsupervised feature learning for 3d scene labeling," in *2014 IEEE International Conference on Robotics and Automation (ICRA)*, pp. 3050–3057, May 2014.
- [22] N. Silberman and R. Fergus, "Indoor scene segmentation using a structured light sensor," in *2011 IEEE International Conference on Computer Vision Workshops (ICCV Workshops)*, pp. 601–608, Nov 2011.